

ZnSe Nanoparticles Reinforced Biopolymeric Soy Protein Isolate Film

Rakesh Kumar^{1,*}, Reshma Praveen¹, Shikha Rani¹, K. Sharma², K. P. Tiwary^{3,*} and K. Dinesh Kumar⁴

¹Department of Biotechnology, Central University of South Bihar, Gaya, India.

²Department of Applied Chemistry, Birla Institute of Technology Mesra, Patna Campus, Patna, India.

³Department of Applied Physics, Birla Institute of Technology Mesra, Patna Campus, Patna, India.

⁴Department of Materials Science & Engineering, Indian Institute of Technology, Patna, India.

*Corresponding Authors: Rakesh Kumar. Email: krrakesh72@gmail.com; rakeshkr@cusb.ac.in; K. P. Tiwary. Email: kptiwary@gmail.com; kptiwary@bitmesra.ac.in.

Abstract: ZnSe nanoparticles have been synthesized by microwave assisted method by using zinc chloride, selenium powder and ethylene diamine. The synthesized nanoparticles have been characterized structurally by FT-IR and XRD as well as morphological characterization was done by scanning electron microscope (SEM). The crystallite size after synthesis was obtained around 30 nm for pure ZnSe nanocrystallites. However, from SEM micrograph, agglomerated ZnSe nanoparticles of irregular shapes were observed. The as-synthesized ZnSe nanoparticles at different contents (1 to 5% w/w w.r.t SPI) were incorporated into soy protein isolate (SPI) to produce reinforced SPI films by solution casting method. The ZnSe nanoparticles incorporated SPI suspensions were subjected to molecular mass and specific conductivity studies. Neat and ZnSe nanoparticles incorporated SPI films were structurally and mechanically characterized by FT-IR and tensile properties, respectively. Transmittance and water uptake studies were also carried out for ZnSe nanoparticles incorporated SPI films. The tensile strength and modulus increased from 5.80 MPa to 10.06 MPa and 18.84 MPa to 94.70 MPa with the increase in the contents of ZnSe nanoparticles from 0 to 5%. Moreover, the results also revealed a good antibacterial effect in ZnSe nanoparticles incorporated SPI film. The main application of nanoparticles incorporated SPI film will be in the area of biodegradable packaging.

Keywords: Soy protein isolate; ZnSe nanoparticles; reinforced film; tensile properties; antimicrobial properties

1 Introduction

Heads of both industrialized and emerging nations of the World have reached to a conclusion that the development of environmentally friendly materials is the need of an hour. Thus, protein-based “green” materials have become a research focus in last 20 years because of their high performance, low cost and eco-friendly characteristics [1]. Soy protein isolate (SPI) among all other protein sources possesses good biocompatibility, biodegradability, processability and easy availability [2]. SPI can be easily processed into film in the presence of suitable plasticizers [3]. However, to overcome several limitations of SPI based films, reinforcement by nanomaterials in SPI has been undertaken in recent times. The limitations of SPI based film are generally in terms of low water resistance and low mechanical properties. Additionally, neat SPI based films are more prone to microbial attack. Recently, a review report has been published that shows the antimicrobial properties of SPI film in presence of several acid additives and nanoparticles [4].

Cu and Zn nanocluster as well as silicon oxides nanoparticles have been incorporated in SPI matrices to get the reinforced SPI material with improved properties [5,6]. Carbon nanotubes (CNTs) [7], chitin whiskers [8], layered silicate [9-11], carbon nanoparticles [12] and silica nanoparticles [13] have been explored as reinforcement materials for SPI. In addition to single composite SPI film, Liu et al. has incorporated chitosan and halloysite nanotubes in SPI to fabricate eco-friendly hybrid composite SPI film with high tensile strength [14]. Bionanocrystal in form of starch and cellulose nanocrystal as well as citric acid-modified starch nanoparticles have been incorporated in SPI [15-17].

On the other hand, authors have also generated nanospheres on SPI film to introduce nanolevel effect via in-situ approach. Nanorod arrays have been constructed/generated through surface oxidation in presence of strong alkali [18]. Li and co-workers fabricated CuO hierarchical flower-like structures on SPI [19]. The growth of nanospheres on SPI film has been generated on SPI by immersing SPI film in diphenyl hydroxyl ethanoic acid (DPHEAc) solution [20]. Xie et al. demonstrated the formation of $\text{Cu}_3(\text{PO}_4)_2 \cdot 3\text{H}_2\text{O}$ nanoflowers on the surface of the SPI film by immersing neat SPI film into a CuSO_4 solution for 10 h similar to the approaches adopted by Kumar et al. for the formation of nanospheres [21].

Zinc selenide (ZnSe) is an important semiconductor material. The various methods used for the synthesis of nanoparticles of ZnSe are co-precipitation method [22], reverse micelle synthesis [23], microwave heating method [24], etc. Microwave irradiation is one of the novel methods and is being considered as new emerging area of research. Recently, microwave treatment at high temperature and pressure was used to prepare heterojunctions of MoS_2 having 2D and 3D structures [25]. This technique was chosen in this work due to its simplicity and potentiality for being adapted to industrial synthesis of nanoparticles. It requires very short reaction time and capable of producing nanoparticles of high purity. The synthesis of ZnSe nanoparticles by microwave irradiation is generally done in aqueous dispersion due to the fact that water has a very high dipole moment. During the formation of the nanoparticles by microwave irradiation, solvents can have an important influence on the size and morphology of the final products. ZnSe nanoparticles have been incorporated in the synthetic polymer such as ethylene vinyl acetate (EVA) polymer to alter the properties of the polymeric films [26].

This study attempts to synthesize ZnSe nanoparticles by microwave technique and characterize it. The as-synthesized ZnSe nanoparticles were then incorporated into the SPI suspension to fabricate ZnSe nanoparticles incorporated SPI films by solution casting method. Molecular mass and conductivity studies of ZnSe nanoparticles incorporated SPI suspension were also carried out. The ZnSe nanoparticles incorporated SPI films were characterized by FT-IR, mechanical, thermomechanical, transmittance and water uptake studies in addition to antimicrobial studies. The development of SPI based materials is considered as potential substitutes for existing petroleum-based synthetic polymers which can not only solve the “white pollution” problem but also ease the over dependence on petroleum resource.

2 Materials and Methods

2.1 Materials

Zinc chloride (ZnCl_2), selenium powder and ethylenediamine of AR grade were purchased from Molychem, Mumbai, India and were used without further purification. Soy protein isolate with a protein content of 90.27% (on dry basis) was provided by Zhengzhou Ruikang Enterprise Co., Ltd. (Zhengzhou, China). Glycerol, sodium chloride and sodium hydroxide pellets were purchased from Fisher Scientific and Titan Biotech Ltd. respectively. *E. Coli* /BL21 strain was procured from G biosciences. Luria Bertani (LB) powder was purchased from HiMedia.

2.2 Synthesis of ZnSe Nanoparticles

Microwave assisted solvothermal method was used for preparation of ZnSe nanoparticles. In the first step, 0.2 g of selenium powder was put into a 50 ml beaker, which was filled with ethylenediamine (en) up to 85% of its total volume. The prepared solution of selenium and ethylenediamine was put on a magnetic stirrer at 70°C with 600-650 rpm for 2 h to produce brown colored homogeneous solution of selenium and ethylenediamine. In the second step, the aqueous solution of ZnCl_2 was mixed with

homogeneous solution of selenium and ethylenediamine. The total volume was made up to 300 ml which was taken in a 500 ml glass beaker and then it was placed on a magnetic stirrer for 30 min at 160°C with 650 RPM. Then the beaker containing resulting solution was put in to microwave oven (LG make) with a maximum power of 900W. The sample was microwave processed for a period of 16 min with a duty cycle of 25%. It means the solution was microwave irradiated for a period of 20 s followed by a rest period of 60 s, which completes one cycle. Around 12 cycles took place to form the nanoparticles of ZnSe. The prepared sample was filtered out and dried in an oven for 10 h at 70°C to get ZnSe nanoparticles.

2.3 Preparation of SPI Film

SPI film was prepared by solution casting method. In the typical method, 1.05 gm of glycerol (30 % w/w with respect to SPI) was added to 50 ml distilled water and the pH of the solution was adjusted around 10.5 by using 1N NaOH. Subsequently, 3.5 gm of SPI was added and subjected to continuous stirring at 60°C for 1 h. The resulting solution was kept overnight in a vacuum desiccator to remove the air bubbles. The solution was then poured on the glass plates of 15 cm × 10 cm and kept at 50-60°C for 24 h. After the designated time, the dried film of about 0.25 ± 0.03 mm was kept at a RH of 75% and subsequently it was peeled off from the glass plates.

2.4 Preparation of ZnSe Nanoparticles Incorporated SPI Film

Different amounts of ZnSe nanoparticles (1 to 5 % w/w w.r.t to SPI) was first sonicated and then added to the as-prepared SPI solution (the pH of the solution decreased to about 7). For sonication, 40% amplitude frequency for 5 min, with 30 s on and 30 s off pulse have been used. That means sonication process was completed with 5 on pulse and 5 off pulse. Final pH of the ZnSe nanoparticles incorporated SPI solution was maintained around 10.5 by the addition of 1N NaOH and was stirred continuously at 60°C for 30 min. The resulting solution was kept overnight in a vacuum desiccators to remove the air bubbles. The solution was then poured on the glass plates and kept at 50-60°C for 24 h. After the designated time, the dried film was kept at a RH of 75% and subsequently it was peeled off from the glass plates. The resulting ZnSe nanoparticles incorporated SPI films were coded as S-0ZnSe, S-1ZnSe, S-2ZnSe, S-3ZnSe, S-4ZnSe and S-5ZnSe where the numeral with ZnSe denotes the content of ZnSe nanoparticles with respect to SPI.

2.5 Molecular Mass Profiles of ZnSe Nanoparticles Incorporated SPI by SDS-PAGE

To study the molecular mass pattern of soy protein, 200 µL of neat and ZnSe nanoparticles incorporated SPI liquid samples were 10 times diluted and was dissolved in 50 µL of loading dye (containing 250 mM Tris-Cl, 10% (w/v) SDS, 40% glycerol, 10 mM dithiothreitol, 0.05% (w/v) bromophenol blue). The mixture was boiled for 10 min and then centrifuged at 13000 rpm for 1 min. Supernatant (10 µL of each protein samples) was loaded in each well. Electrophoresis was performed at a constant voltage of 100V for stacking and 120V for separation. The gel was stained with Coomassie Brilliant Blue-R250 and destained with solution containing 10% glacial acetic acid and 40% methanol.

2.6 Antimicrobial Studies

SPI film with a dimension of 1 cm × 1 cm were placed on the surface of Luria Bertani (LB) agar plate, which has been previously spreaded with *E. coli* /BL21 strain (60 µL). The plates were incubated at 37°C for overnight and the growth of bacteria on SPI film were observed for 5 days.

2.7 Characterizations of ZnSe Nanoparticles

The structural properties of the synthesized ZnSe nanoparticles were analyzed by recording the XRD pattern by model Bruker AXS D8 Advance with Cu K α radiation having wavelength 1.5406 Å. The crystallite size of nanoparticles was measured by Debye-Scherrer formula which is given as

$$D = \frac{0.9\lambda}{\beta \cos\theta}$$

where λ is the wavelength of X-ray, β is called FWHM (Full Width at Half Maxima), θ is the angle of diffraction.

SEM characterization of ZnSe nanoparticles was made by JEOL Japan, Model JSM-6390LV at CUSSET Kochi, India. FT-IR spectrum of ZnSe nanoparticles were recorded by Spectroscopy model Thermo Nicolet, Avatar 370 within range 4000-400 cm^{-1} at resolution 4 cm^{-1} at CUSSET Kochi, India.

2.8 Characterizations of ZnSe Nanoparticles Incorporated SPI Suspension and Film

2.8.1 Specific Conductivity

Specific conductivity was performed on a Conductivity Meter 304 (Systronic, India). The neat and ZnSe nanoparticles incorporated liquid SPI suspension samples were diluted 10 times and conductivity was measured at 30°C. Here, 0.01N KCl was taken as standard which has the known specific conductivity of 1.55 mMHOS at 30°C.

2.8.2 Color and Transparency

The color of the neat and ZnSe nanoparticles incorporated SPI film samples were determined by visual inspection. To evaluate transparency, the film samples were cut to the exact dimension of the side of a glass cuvette and then mounted onto the inside of the cuvette. The transparency of the film samples was expressed in terms of transmittance measured at 400 and 700 nm using a UV-vis spectrophotometer (Motras Scientific). An empty cuvette was used as a blank.

2.8.3 FT-IR

Fourier transform infrared spectra (FT-IR) of the neat and ZnSe nanoparticles incorporated SPI film samples were carried out on FT-IR spectrophotometer (from Perkin-Elmer, USA) at IIT Patna, India in the range of wavenumber varying from 4000 to 400 cm^{-1} . All spectra were reported after an average of 32 scans.

2.8.4 Tensile Strength

The tensile strength, tensile modulus and elongation at break values of the neat and ZnSe nanoparticles incorporated SPI film samples were measured on a Universal Tensile Testing machine (from Zwick, Germany) at IIT Patna, India, with a tensile rate of 10 mm/min according to ASTM D 882. The tensile specimens with dimension of 80 mm \times 10 mm and thickness of \sim 0.2 mm were prepared by casting and an average value from five replicates of each sample was taken.

2.8.5 DMTA

Dynamic mechanical thermal analysis (DMTA) of the neat and ZnSe nanoparticles incorporated SPI film samples was performed on a dynamic mechanical analyzer (DMA8000, PerkinElmer, Buckinghamshire, UK) at IIT Patna with dual cantilever at a frequency of 1 Hz. The films of 50 mm \times 10 mm (length \times width) in dimensions were tested at temperatures ranging from -50 to 250°C with a heating rate of 2 $^{\circ}\text{C min}^{-1}$.

2.8.6 Water Uptake

The water uptake of neat and ZnSe nanoparticles incorporated SPI films were evaluated according to ASTM D570-81. The films were cut in small square pieces (1 cm \times 1 cm) in duplicate and kept at 60°C for a period of 24 h. It was cooled in a desiccator and weighed (W_0). The film pieces were then immersed

in 15 ml distilled water for 24 h. The films were dried with tissue paper to remove the excess water from the surface and weighed (W_1). The water uptake of the films was calculated as follows:

$$\text{Water Uptake}(\%) = \frac{W_1 - W_0}{W_0} \times 100$$

3 Results and Discussions

3.1 Characterization of ZnSe Nanoparticles

The SEM image is used for observing the morphological property of as-prepared ZnSe nanoparticles and the micrograph is shown in Fig. 1. The SEM image shows that ZnSe nanoparticles are composed of spherical and rectangular shaped agglomerations with an average diameter of 1-2 μm similar to that reported by Helal et al. [27]. The image also revealed that the as-fabricated ZnSe nanoparticles consisted of irregular shaped particles. It has been reported by Helal et al. that the average particle size in nano level can be estimated by transmission electron microscopy (TEM) or XRD technique.

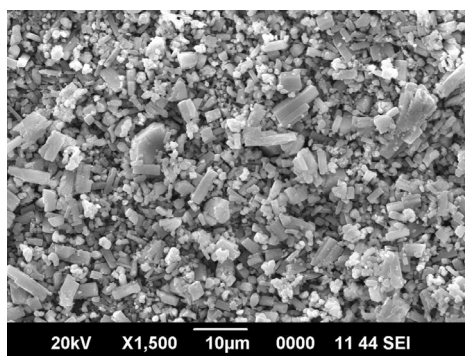


Figure 1: SEM photograph of ZnSe nanoparticles

In this research paper, we have used XRD to estimate the average particle size of ZnSe nanoparticles. The XRD pattern peaks were indexed for the cubic phase of ZnSe as shown in Fig. 2. The crystallite size was found to be around 30 nm for ZnSe nanoparticles by Debye-Scherrer formula.

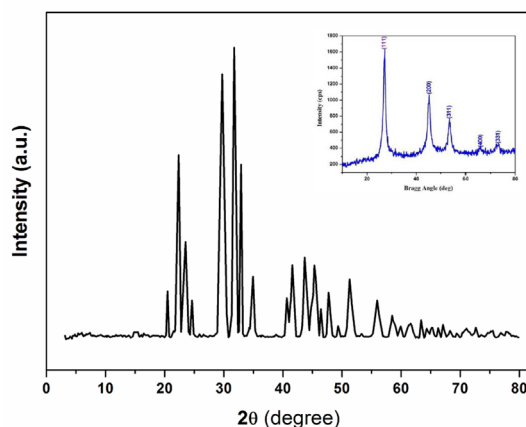


Figure 2: XRD of ZnSe nanoparticles. In inset is the XRD pattern of ZnSe nanoparticles as reported in [28]

Fig. 3 illustrates the FT-IR spectrum of ZnSe nanoparticles. The peak at 3286 cm^{-1} was assigned to O-H stretching. However, the peak at 1169 cm^{-1} observed on ZnSe corresponded to the Se-O stretching

bond and the one that appearing at 973 cm^{-1} represented the characteristics absorption peak of ZnSe which corresponds to the ZnSe stretching bond similar to that observed for ZnS nanoparticles [28,29].

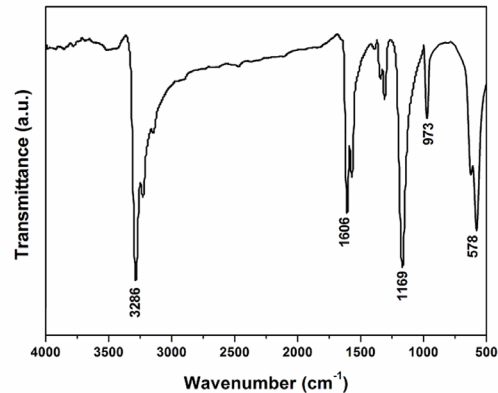


Figure 3: FT-IR spectra of ZnSe nanoparticles

3.2 SDS-PAGE of Neat and ZnSe Nanoparticles Incorporated SPI Suspension

Fig. 4(a) represents the molecular mass profile of SPI in presence of molecular mass marker [30]. Protein composition of neat and ZnSe nanoparticles incorporated liquid SPI samples was analyzed by SDS-PAGE which showed mixture of high and low molecular mass proteins in the form of a continuous band in the gel as shown in Fig. 4(b). However, two distinct molecular mass fractions of 34-38 and ~68 kDa were resolved which signified that the protein fraction of these molecular masses were predominant in soy protein [30]. The band of very high intensity at 35-39 kDa represented the acidic subunit of 11S-RG protein. α , $\alpha 1$ and β subunit of 7S-RG are denoted by ~80, ~68 and ~48 kDa molecular mass bands, respectively. There is no major difference in the molecular mass band of SPI after incorporation of ZnSe nanoparticles in it.

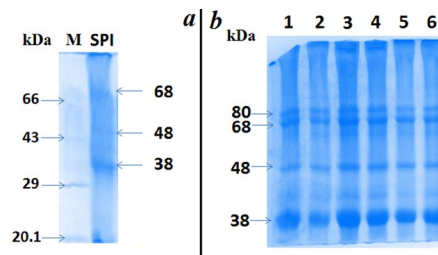


Figure 4: SDS-PAGE analysis for (a) 10 μl of neat SPI samples (b) ZnSe nanoparticles incorporated SPI suspension (10 times diluted). Numbers on left are the molecular masses of marker proteins in kDa and M is marker proteins

3.3 Specific Conductivity of Neat and ZnSe Nanoparticles Incorporated SPI Suspension

Fig. 5 shows the percentage change in specific conductivity with respect to contents of ZnSe nanoparticles. The neat SPI liquid sample demonstrated the specific conductivity of 6.1 mMHOs when 0.01N KCl was taken as standard at 30°C . The specific conductivity gradually increased to 36.06% with the introduction of 1% ZnSe nanoparticles in the liquid SPI samples. Thus, with the % increase in ZnSe nanoparticles, the specific conductivity also got increased, except for S-2ZnSe which showed the lowest increase. Since ZnSe is charged particle and the decrease in specific conductivity value for S-2ZnSe may indicate high interaction between oppositely charged moieties of SPI and ZnSe nanoparticles.

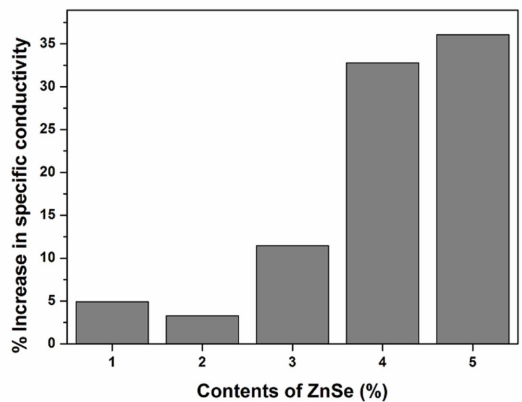


Figure 5: Specific conductivity of ZnSe nanoparticles incorporated SPI films

3.4 Visual Inspection and Transmittance of Neat and ZnSe Nanoparticles Incorporated SPI Films

The neat SPI film was yellow in colour, which changed to blackish when incorporated with ZnSe nanoparticles. The intensity of black colour increased with the increase in the amount of ZnSe nanoparticles. From visual inspection, it was evident that sonicated ZnSe nanoparticles in SPI films exhibited evenness in the surface while non-sonicated ZnSe nanoparticles showed clump formation in the films. Tab. 1 shows the dependence of the transmittance on the ZnSe nanoparticles content in the SPI films. The neat SPI film demonstrated the transmittance of 36.77% and 36.79% at 400 nm and 700 nm, respectively. However, with the introduction of ZnSe nanoparticles in the SPI films, the transmittance decreased when compared to S-0ZnSe. On contrary, the transmittance of S-3ZnSe increased when compared to S-1ZnSe and this may be attributed to uniform dispersion of ZnSe nanoparticles at this content in SPI.

Table 1: Transmittance and photograph of neat and ZnSe nanoparticles incorporated SPI films at 400 nm and 700 nm

Sample Designation	Photograph of film	Transmittance (%) at	
		400 nm	700 nm
S-0ZnSe		36.77	36.79
S-1ZnSe		31.65	31.08
S-2ZnSe		23.76	22.86
S-3ZnSe		48.93	45.12
S-4ZnSe		13.41	14.26
S-5ZnSe		9.41	11.55

3.5 FT-IR Spectrum of Neat and ZnSe Nanoparticles Incorporated SPI Films

Fig. 6 shows the FT-IR spectra of the neat and ZnSe nanoparticles incorporated SPI films. A broad N-H stretching and O-H stretching band assigned to amide A of soy protein films was observed between 3200 and 3400 cm^{-1} in neat SPI films (S-0ZnSe) [30]. Similar to earlier report, the amide II and amide III bands of soy protein were observed at 1545 and 1236 cm^{-1} , respectively [30,31]. The carbonyl band (C=O) in soy protein was observed at 1639 cm^{-1} . With the increase in the contents of ZnSe nanoparticles, the broadness of the peak between 3200 and 3400 cm^{-1} decreased and this signified the decrease in hydrophilicity of ZnSe nanoparticles incorporated SPI films. However, the two extra peaks observed for ZnSe nanoparticles incorporated SPI film corresponded to the Se-O stretching bond that shifted from 1169 cm^{-1} (Fig. 3) to 1265 cm^{-1} and the other ZnSe stretching bond that appeared at 973 cm^{-1} (Fig. 3) now shifted to 805 cm^{-1} [32].

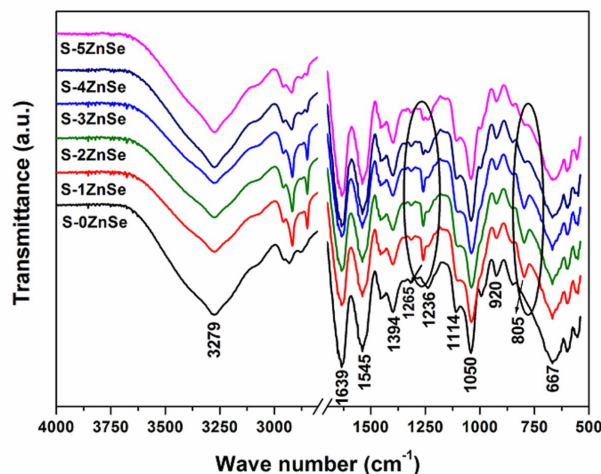


Figure 6: FT-IR spectrum of ZnSe nanoparticles incorporated SPI films

3.6 Mechanical Properties of Neat and ZnSe Nanoparticles Incorporated SPI Films

Tab. 2 shows the mechanical properties of ZnSe nanoparticles incorporated SPI films. The tensile strength and modulus of the neat SPI sample were about 5.80 ± 0.65 MPa and 18.85 ± 14.31 MPa, respectively. The elongation at break for neat SPI sample was 102.07 ± 19.32 %. As the content of ZnSe nanoparticles increased from 1 to 5%, the tensile strength increased, whereas the elongation at break decreased. The modulus exhibited an increase with increasing content of ZnSe nanoparticles. With increasing ZnSe nanoparticles content from 1-5%, the behavior of the SPI films changed from flexible to brittle. The tensile strength and modulus of the S-1ZnSe sample were about 5.97 ± 0.43 MPa and 38.52 ± 4.55 MPa, respectively, whereas those of the S-5ZnSe film, were about 10.06 ± 1.80 MPa and 94.70 ± 0.50 MPa, respectively. S-5ZnSe sample showed a very low elongation at break (17.63 ± 6.70 %). The three mechanical parameters showed similar changes as was observed for SPI at increasing MWNTs content [32]. In the whole ZnSe nanoparticles content range, the elongation at break kept decreasing with the increase of the ZnSe nanoparticles addition.

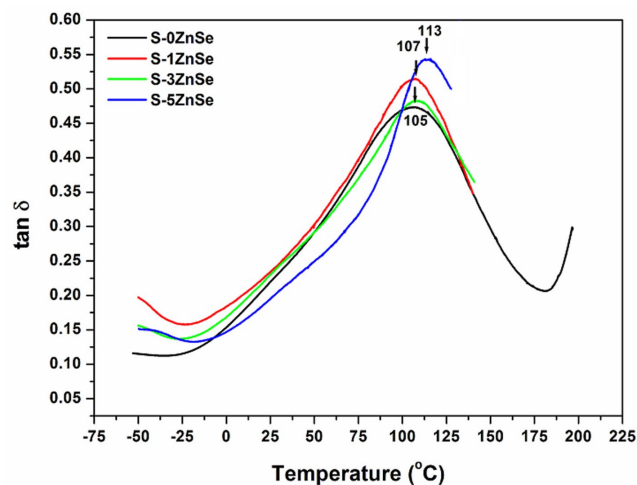
Since SPI film is formed at alkaline pH hence there will be presence of negative charges as shown in specific conductivity studies as stated in Section 3.3. High positive charges (acidic pH) or high negative charges (alkaline pH) favor the film forming ability of SPI suspension [33]. From the conductivity studies, as discussed in Section 3.3, the percentage increase in overall charges for S-2ZnSe was lowest indicating low overall charges of S-2ZnSe suspension. Hence, the significant decrease in tensile strength and tensile modulus for S-2ZnSe may be attributed to reduced film forming ability of S-2ZnSe composition as compared to other compositions of ZnSe nanoparticles incorporated SPI film.

Table 2: Mechanical properties of neat and ZnSe nanoparticles incorporated SPI films

Sample Name	Tensile strength at break (MPa)	Elongation at break (%)	Youngs' Modulus (MPa)
S-0ZnSe	5.80 ± 0.65	102.07 ± 19.32	18.85 ± 14.31
S-1ZnSe	5.97 ± 0.43	85.01 ± 2.00	38.52 ± 4.55
S-2ZnSe	3.70 ± 1.17	26.47 ± 4.92	30.16 ± 1.38
S-3ZnSe	5.20 ± 1.72	33.76 ± 6.01	42.55 ± 12.77
S-4ZnSe	7.64 ± 0.06	27.89 ± 1.71	54.25 ± 2.55
S-5ZnSe	10.06 ± 1.80	17.63 ± 6.70	94.70 ± 0.50

3.7 DMA of Neat and ZnSe Nanoparticles Incorporated SPI Films

Fig. 7 shows the temperature dependence of the loss factor ($\tan \delta$) of the neat and ZnSe nanoparticles SPI films. The α -relaxation (T_α) values attributed to the protein-rich domains for neat SPI was observed at 105°C. With the increase in the content of ZnSe nanoparticles from 1 to 5% the value of T_α increased from 107 to 113°C indicating the decrease in the molecular mobility of the protein materials [3]. There was significant increase in damping for ZnSe nanoparticles incorporated SPI film as compared to neat SPI film, and interestingly, S-5ZnSe showed highest damping. The material failure at 148°C was observed for S-1ZnSe nanoparticles incorporated SPI film which decreased to 127°C for S-5ZnSe.

**Figure 7:** Tan delta curve of ZnSe nanoparticles incorporated SPI films

The storage modulus curves of the ZnSe nanoparticles incorporated SPI films are presented in Fig. 8. The storage modulus of neat and ZnSe nanoparticles incorporated SPI films decreased with the increase in temperature. S-5ZnSe samples showed highest storage modulus. Overall, it was observed that there was increase in storage modulus of the SPI film after the incorporation of ZnSe nanoparticles. Storage moduli results confirmed that the storage modulus of ZnSe nanoparticles incorporated SPI film increased on reinforcements with nanoparticles. Interestingly, a hump was observed for all the ZnSe nanoparticles incorporated SPI and that hump increased with the increase in the contents of ZnSe nanoparticles in SPI.

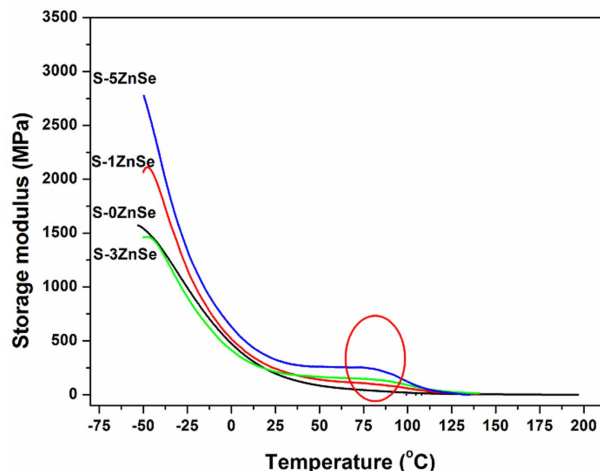


Figure 8: Storage modulus of ZnSe nanoparticles incorporated SPI films

3.8 Water Uptake of Neat and ZnSe Nanoparticles Incorporated SPI Films

Fig. 9 shows the water uptake properties of neat and ZnSe nanoparticles incorporated SPI films. Soy protein film without ZnSe nanoparticles (S-0ZnSe) showed high water uptake ($279.65 \pm 15.64\%$) which drastically decreased to $73.59 \pm 17.18\%$ at S-5ZnSe. However, the water uptake for S-1ZnSe, S-2ZnSe, S-3ZnSe, S-4ZnSe were almost same within the error limit. Similarly, the multiwalled carbon nanotubes-soy protein isolate composite plastics (MWNTs/SPI) displayed lower water uptake values than the neat soy protein plastics [34]. The neat soy protein plastics with glycerol plasticizer possessed high water absorption for large amount of polar groups on the protein macromolecular chains as well as the high hydrophilicity of glycerol plasticizer. With the increase of ZnSe nanoparticles from 0 to 5%, the water uptake value decreased.

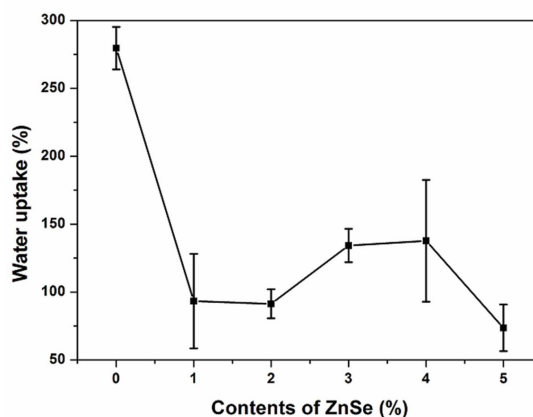


Figure 9: Water uptake of ZnSe nanoparticles incorporated SPI films

3.9 Antimicrobial Properties of Neat and ZnSe Nanoparticles Incorporated SPI Films

There was no antibacterial property contributed by S-0ZnSe and S-1ZnSe. However, at higher % of ZnSe (2-5%), designated as S-2ZnSe, S-3ZnSe, S-4ZnSe, S-5ZnSe showed good antibacterial property as there was no microbial growth on the films after 24 h, as shown in Fig. 10. The same antimicrobial effect was observed till 5 days of incubation. Similarly, it has been reported that the commendable antimicrobial activity of the composite relays on the presence of nanoZnO particles in the matrix where Zn^{2+} ions attack the negatively charged cell wall and will lead to leakage and ultimately in death of bacteria [35].

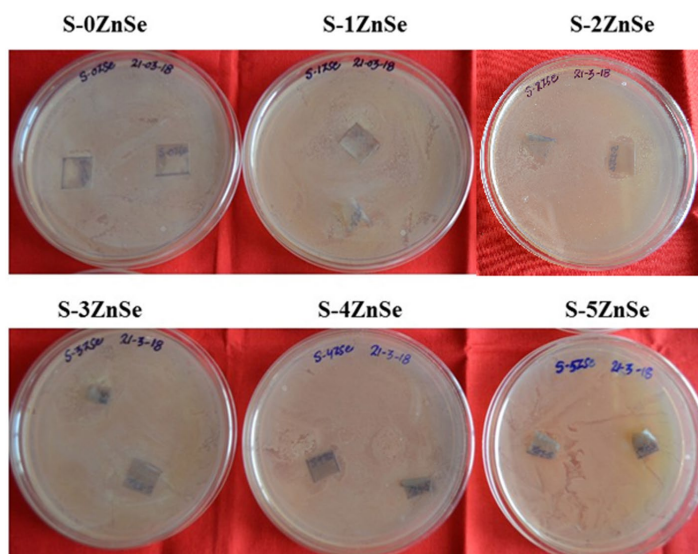


Figure 10: Microbial growth on ZnSe nanoparticles incorporated SPI films

4 Conclusions

Different contents of ZnSe nanoparticles (0-5%) were successfully incorporated in SPI to prepare light yellow to dark grey homogeneous SPI films. The SDS-PAGE image of the gel showed the clear molecular mass bands without any change in molecular mass profile of soy protein after incorporation of ZnSe nanoparticles. The tensile strength at break, tensile modulus and storage modulus increased with the increase in the content of ZnSe nanoparticles. However, elongation at break decreased with increasing ZnSe nanoparticles content. The value of tan delta increased upon incorporation of ZnSe nanoparticles which indicated restricted molecular mobility of protein molecules and that can be correlated with low elongation at break. The percentage of water uptake decreased significantly with the increase in content of ZnSe nanoparticles indicating less hydrophilic character of the nanoparticles incorporated SPI film. No growth of *E. coli* on the surface of ZnSe nanoparticles incorporated SPI films (at high contents) suggested the antibacterial nature of the SPI films. Thus, ZnSe nanoparticles as a reinforcement nanomaterial for SPI could improve their mechanical and water resistance properties compared to neat soy protein film.

Note: A part of the paper entitled ‘Influence of Mg on Structural and Optical Properties of ZnSe Nanocrystals Synthesized by Microwave Assisted Technique’ has been presented in a conference ISFM-18 (International Symposium on Functional Materials (ISFM-2018): Energy and Biomedical Applications) and submitted for publication as conference proceedings.

References

1. Wu, Q., Sakabe, H., Isobe, S. (2003). Processing and properties of low cost corn gluten meal/wood fiber composite. *Industrial & Engineering Chemistry Research*, 42, 6765-6573.
2. Li, Y. D., Zeng, J. B., Wang, X. L., Yang, K. K., Wang, Y. K. (2008). Structure and properties of soy protein/poly butylene (succinate) blends with improved compatabilty. *Biomacromolecules*, 9, 3157-3164.
3. Kumar, R. Wang, L., Zhang, L (2009). Structure and mechanical properties of soy protein materials plasticized by thiodiglycol. *Journal of Applied Polymer Science*, 111, 970-977.
4. Rani, S., Kumar, R. (2019). A review on material and antimicrobial properties of soy protein isolate film. *Journal of Polymers and the Environment*, 27(8), 1613-1628.
5. Li, K., Chen, H., Li, Y., Li, J., Hen, J. (2015). Endogenous Cu and Zn nanocluster-regulated soy protein isolate films: excellent hydrophobicity and flexibility. *RSC Advances*, 5, 66543-66548.

6. Ai, F., Zheng, H., Wei, M., Huang, J. (2007). Soy protein plastics reinforced and toughened by SiO₂ nanoparticles. *Journal of Applied Polymer Science*, 105, 1597-1604.
7. Moniruzzaman, M., Winey, K. I. (2006). Polymer nanocomposites containing carbon nanotubes. *Macromolecules*, 39, 5194-5205.
8. Zheng, H., Tan, Z., Zhan, Y., Huang, J. (2003). Morphology and properties of soy protein plastics modified with chitin. *Journal of Applied Polymer Science*, 90, 3676-3682.
9. Chen, P., Zhang, L. (2006). Interaction and properties of highly exfoliated soy protein/montmorillonite nanocomposites. *Biomacromolecules*, 7, 1700-1706.
10. Yu, J., Cui, G., Wei, M., Huang, J. (2007). Facile exfoliation of rectorite nanoplatelets in soy protein matrix and reinforced bionanocomposites thereof. *Journal of Applied Polymer Science*, 104, 3367-3377.
11. Tian, H., Guo, G., Fu, X., Yao, Y., Yuana, L. et al. (2018). Fabrication, properties and applications of soy-protein-based materials: a review. *International Journal of Biological Macromolecules*, 120, 475-490.
12. Li, Y., Chen, H., Dong, Y., Li, K., Li, L. et al. (2016). Carbon nanoparticles/soy protein isolate bio-films with excellent mechanical and water barrier properties. *Industrial Crops and Products*, 82, 133-140.
13. Tian, H. (2002). Processing and properties of soy protein/silica nanocomposites fabricated in situ synthesis. *Journal of Composite Materials*, 46, 427-435.
14. Liu, X., Song, R., Zhang, W., Qi, C., Zhang, S. et al. (2017). Development of eco-friendly soy protein isolate films with high mechanical properties through HNTs, PVA, and PTGE synergism effect. *Scientific Reports*, 7, 44289.
15. González, A., Alvarez Igarzabal, C. I. (2015). Nanocrystal-reinforced soy protein films and their application as active packaging. *Food Hydrocolloids*, 43, 777-784.
16. Xie, D. Y., Quian, D., Song, F., Wang, X. L., Wang, Y. Z. (2017). A fully biobased encapsulant constructed of soy protein and cellulose nanocrystals for flexible electromechanical sensing. *ACS Sustainable Chemistry & Engineering*, 5, 7063-7070.
17. Tian, H., Xu, G. (2011). Processing and characterization of glycerol-plasticized soy protein plastics reinforced with citric acid-modified starch nanoparticles. *Journal of Polymers and the Environment*, 19, 582-588.
18. Chen, X., Kong, L., Dong, D., Yang, G., Yu, L. et al. (2009). Fabrication of functionalized copper compound hierarchical structure with bionic superhydrophobic properties. *The Journal of Physical Chemistry C*, 113, 5396-5401.
19. Li, H., Yu, S., Han, X. (2016). Fabrication of CuO hierarchical flowerlike structures with biomimetic superamphiphobic, self-cleaning and corrosion resistance properties. *Chemical Engineering Journal*, 83, 1443-1454.
20. Kumar, R., Zhang, L. (2008). Water-induced hydrophobicity of soy protein materials containing 2, 2-diphenyl-2-hydroxyethanoic acid. *Biomacromolecules*, 9, 2430-2437.
21. Xie, W. Y., Song, F., Wang, X. L., Wang, Y. Z. (2017). Development of copper phosphate nanoflowers on soy protein toward a superhydrophobic and self-cleaning film. *ACS Sustainable Chemistry & Engineering*, 5, 869-875.
22. Iranmanesha, P., Saeedniab, S., Nourzpoor, M. (2015). Characterization of ZnS nanoparticles synthesized by co-precipitation method. *Chinese Physics B*, 24, 46-104.
23. Eastoe, J., Hollamby, M. J., Hudson, L. (2006). Recent advances in nanoparticle synthesis with reversed micelles. *Advanced Colloid Interface Science*, 128-130, 5-15.
24. Shkir, M., Kushwaha, S. K., Maurya, K. K., Wahab, M. A. (2009). Characterization of ZnSe nanoparticles synthesized by microwave heating process. *Solid State Communication*, 149(45-46), 2047-2049.
25. Balati, A., Wagle, D., Nash, K. L., Shipley, H. J. (2019). Heterojunction of TiO₂ nanoparticle embedded into ZSM5 to 2D and 3D layered-structures of MoS₂ nanosheets fabricated by pulsed laser ablation and microwave technique in deionized water: structurally enhanced photocatalytic performance. *Applied Nanoscience*, 9(1), 19-32.
26. Sebastian, J., Thachil, E. T., Mathen, J. J., Edakkara, A. J., Kuriakose, N. et al. (2015). Preparation and characterization of ZnSe/EVA nanocomposites for photovoltaic modules. *Journal of Minerals and Materials Characterization and Engineering*, 3, 215-224.
27. Helal, E. H. D., Dessouki, H. A., Nassar, M. Y., Ahmed, I. S. (2018). Preparation and spectral analysis of nano sized ZnSeparticles. *Journal of Basic and Environmental Sciences*, 5, 20-24.

28. Ahamed, A. J., Ramar, K., Kumar, P. V. (2016). Synthesis and characterization of ZnSe nanoparticles by co-precipitation method. *Journal of Nanoscience and Technology*, 2(3), 148-150.
29. Tiwary, K. P., Choubey, S. K., Sharma, K. (2013). Structural and optical properties of ZnS nanoparticles synthesized by microwave irradiation method. *Chalcogenide Letters*, 10, 319-323.
30. Kumar, R., Rani, P., Kumar, K. D. (2019). Soy protein isolate film by incorporating mandelic acid as well as through fermentation mediated by *Bacillus Subtilis*. *Journal of Renewable Materials*, 7, 103-115
31. Insaward, A., Duangmal K., Mahawanich, T. (2015). Mechanical, optical, and barrier properties of soy protein film as affected by phenolic acid addition. *Journal of Agricultural and Food Chemistry*, 63, 9421-9426.
32. Mubashshir, M., Farooqi, H., Srivastava, K. (2014). Structural, optical and photoconductivity study of ZnS nanoparticles synthesized by a low temperature solid state reaction method. *Materials Science in Semiconductor Processing*, 20, 61-67.
33. Xiang, A., Guo, G., Tian, H. (2017). Fabrication and properties of acid treated carbon nanotubes reinforced soy protein nanocomposites. *Journal of Polymers and the Environment*, 25, 519-525.
34. Guo, G., Tian, H., Wu, Q. (2019). Influence of pH on the structure and properties of soy protein/montmorillonite nanocomposite prepared by aqueous solution intercalating. *Applied Clay Science*, 171, 14-19.
35. Zhang, Z. Y., Xiong, H. M. (2015). Photoluminescent ZnO nanoparticles and their biological applications. *Materials (Basel)*, 8, 3101-3127.